

Orbital textures and charge density waves: towards orbitronics in transition metal dichalcogenides

T. Ritschel,^{1,2} J. Trinckauf,¹ K. Koepf, ¹ B. Büchner,^{1,2}
M. v. Zimmermann,³ H. Berger,⁴ Y. I. Joe,⁵ P. Abbamonte,⁵ and J. Geck¹

¹Leibniz Institute for Solid State and Materials Research IFW Dresden, Helmholtzstr. 20, 01069 Dresden, Germany

²Institute for Solid State Physics, Dresden Technical University, TU-Dresden, 01062 Dresden, Germany

³Deutsches Elektronensynchrotron DESY, Notkestr. 85, 22603 Hamburg, Germany

⁴Ecole polytechnique Federale de Lausanne, Switzerland

⁵Department of Physics and Frederick Seitz Materials Research Laboratory,
University of Illinois, Urbana, Illinois 61801, USA

Low-dimensional electron systems, as realized naturally in graphene or created artificially at the interfaces of heterostructures, exhibit a variety of fascinating quantum phenomena with great prospects for future applications. [1, 2]. Once electrons are confined to low dimensions, they also tend to spontaneously break the symmetry of the underlying nuclear lattice by forming so-called density waves [3]; a state of matter that currently attracts enormous attention because of its relation to various unconventional electronic properties [4–8]. In this study we reveal a remarkable and surprising feature of charge density waves (CDWs), namely their intimate relation to orbital order. For the prototypical material 1T-TaS₂ we not only show that the CDW within the two-dimensional TaS₂-layers involves previously unidentified orbital textures of great complexity. We also demonstrate that two metastable stackings of the orbitally ordered layers allow to manipulate salient features of the electronic structure. Indeed, these orbital effects enable to switch the properties of 1T-TaS₂ nanostructures from metallic to semiconducting with technologically pertinent gaps of the order of 200 meV. This new type of orbitronics is especially relevant for the ongoing development of novel, miniaturized and ultra-fast devices based on layered transition metal dichalcogenides [9, 10].

Among the various transition metal dichalcogenides (TMDs), 1T-TaS₂ stands out because of its particularly rich electronic phase diagram as a function of pressure and temperature [11]. This phase diagram not only features incommensurate, nearly commensurate and commensurate CDWs, but also pressure-induced superconductivity below 5 Kelvin. In addition to this, it was proposed early on that the low-temperature commensurate CDW (C-CDW), which is illustrated in Fig. 1 (a),(c), also features many-body Mott-physics [12]. Experimental evidence for the presence of Mott-physics in 1T-TaS₂ has indeed been obtained recently by time-resolved spectroscopies, which observed the ultra-fast closing of a charge excitation gap, which has been interpreted as a fingerprint of significant electron-electron interactions [13–15].

Even though the above scenario for the C-CDW is widely accepted, important experimental facts remain to be understood: the very strong suppression of the C-CDW with external pressure is puzzling. Already above 0.6 GPa, the C-CDW is no longer stable, although nesting conditions, band widths as well as the lattice structure remain essentially unchanged. It is also not clear how ordered defects within the C-CDW order, which emerge in the nearly commensurate phase (NC-CDW) upon heating [16, 17] and which do not cause significant changes in the bandwidths, can render U completely ineffective [18]. In the following we will show that all these issues are explained consistently in terms of orbital textures that are intertwined with the CDW. In addition to this, we also demonstrate that this new twist to the physics of

CDWs also provides a new and powerful device concept for future applications based on TMDs.

An important feature of the C-CDW is its partially disordered stacking along the *c*-axis: characterizing the relative alignment of the C-CDW in adjacent *ab*-planes in terms of stacking vectors \mathbf{T}_S , which connect the central Ta-sites in successive layers (cf. Figs. 2 (e) and (f)), the *c*-axis stacking is given by a mixture of $\mathbf{T}_S = \mathbf{1c}$ and the 3 symmetry equivalent $\mathbf{T}_S = 2\mathbf{a} + \mathbf{c}$, $2\mathbf{b} + \mathbf{c}$ and $-2(\mathbf{a} + \mathbf{b}) + \mathbf{c}$ [19, 20]. The effect of the different \mathbf{T}_S on the electronic structure so far remained unexplored. Our highly efficient DFT approach (see methods), however, enables us to study these effects for the first time within the local density approximation (LDA).

For our *ab initio* calculations, we chose two superstructures with $\mathbf{T}_S = \mathbf{1c}$ and $\mathbf{T}_S = 2\mathbf{a} + \mathbf{c}$, respectively, which represent the two metastable types of stacking found experimentally. For both calculations the in-plane modulation was kept the same. Fig. 1 (d) shows the band structures for the C-CDW with $\mathbf{T}_S = \mathbf{1c}$ and the undistorted lattice, where the band dispersions are shown along high symmetry directions of the Brillouin zone of the unmodulated structure (Fig. 1 (b)). In good agreement with previous DFT results [21], the band structure in the plane through Γ , M and K is fully gapped and only along Γ -A a Fermi level crossing occurs. This yields a one-dimensional metal, in-line with recent reports [22]. A major disadvantage of such supercell calculations is, however, that the additional backfolded bands only indicate for which momenta \mathbf{k} and energies ω electronic states ex-

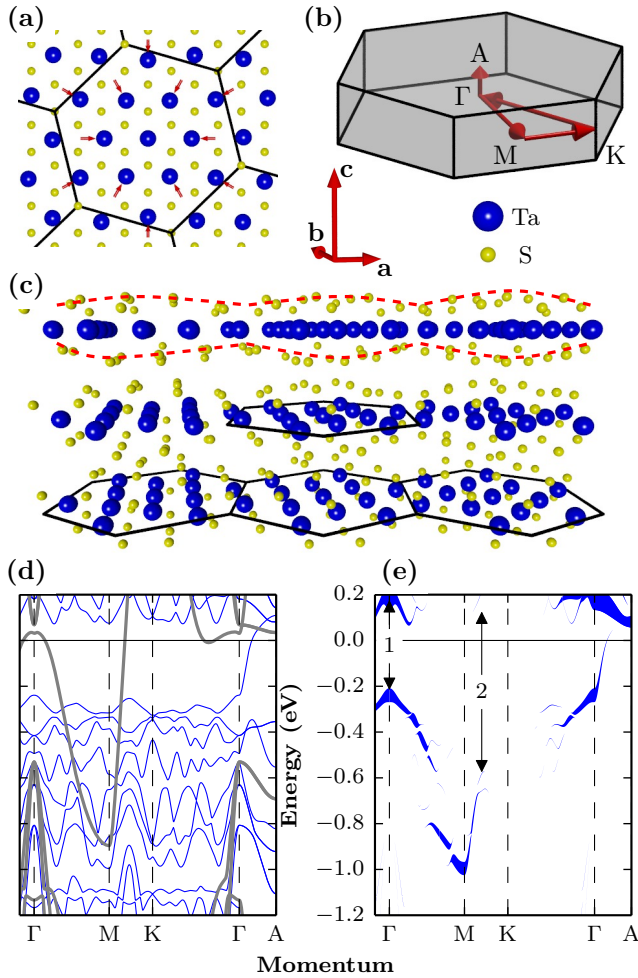


FIG. 1. **The $\sqrt{13} \times \sqrt{13}$ supercell structure of 1T-TaS₂.** (a) and (c): View along the c -axis and parallel to the ab -planes, respectively ($\mathbf{a}, \mathbf{b}, \mathbf{c}$: lattice vectors of the undistorted P3m1 crystal structure). The Ta-displacements indicated by red arrows in (a) are mainly parallel to the ab -planes, resulting in clusters containing 13 Ta-sites. Red dashed lines in (c) highlight the breathing of the S-sites perpendicular to the ab -plane. (d): LDA supercell band structure along the high symmetry direction in the Brillouin zone shown in (b). The gray lines indicate the unreconstructed band structure. (e): The unfolded band structure. The thickness of bands measures the spectral weight at this position. Arrows indicate the gaps at Γ and between M and K which are commonly named Mott-gap (1) and CDW-gap (2), respectively.

ist. There is no information about the occupation of these states. Exactly this information is provided by the so-called spectral function $A(\mathbf{k}, \omega)$ [23], which is the physically relevant quantity that can be accessed experimentally by angle-resolved photoemission spectroscopy (ARPES).

An approximation for $A(\mathbf{k}, \omega)$ within DFT, can be obtained using the so-called unfolding procedure [24]. The result of this unfolding procedure for the band structure shown in Fig.1 (d) is presented in Fig.1 (e), where the

thickness of the individual bands reflects $|A(\mathbf{k}, \omega)|^2$. It is clearly visible that only a small fraction of the reconstructed band structure carries substantial spectral weight. Unlike the bands in Fig.1 (d), the unfolded band structure allows to clearly identify dispersing bands and, correspondingly, the size and location of energy gaps. Specifically, our calculation yields two gaps around the Fermi level E_F , indicated by arrows in Fig.1 (e). The gap at Γ is usually interpreted as a Mott-gap due to the electron-electron interaction U [15, 25]. Between M and K a second gap is formed, which fits well to the Fermi surface nesting vector and is therefore commonly assigned to a CDW-gap due to the electron-phonon coupling. It is very important to note here, that our calculations do not include any onsite interactions U . The fact that the gap at Γ occurs already without including U is therefore remarkable, as it already shows that the gap at Γ is not mainly caused by Mott-physics.

In Fig.2 we compare the unfolded LDA band structures for $\mathbf{T}_S = 1\mathbf{c}$ and $\mathbf{T}_S = 2\mathbf{a} + \mathbf{c}$, which yields the first major result of this study: the dramatic dependence of the electronic structure on the CDW-stacking. As can be observed in Figs.2 (c) and (d), essential features of the low-energy electronic structure depend critically on the stacking. Most notably the bands around the Γ -point are strongly affected. While for $\mathbf{T}_S = 2\mathbf{a} + \mathbf{c}$ the in-plane dispersions show E_F -crossings along Γ -K and Γ -M, both crossings are completely absent for $\mathbf{T}_S = 1\mathbf{c}$. Even the size of the so-called CDW-gap between M-K depends on \mathbf{T}_S , although it prevails for both stackings. Therefore, a transition from an in-plane metal to an in-plane semiconductor occurs as a function of \mathbf{T}_S . Considering that the ab -planes of 1T-TaS₂ are usually thought to realize strongly two-dimensional metallic systems, these are most surprising results.

The comparison of the two DFT models to the ARPES data in Fig.2 (a) shows that the calculation for $\mathbf{T}_S = 2\mathbf{a} + \mathbf{c}$ describes the experiment extremely well for binding energies below -0.3eV . This is consistent with the XRD data in Fig.2(b), which reveals that $\mathbf{T}_S = 2\mathbf{a} + \mathbf{c}$ is indeed dominant. However, it is also obvious that both DFT models fail to describe the electronic states close to E_F and, in particular, the pseudo-gap observed experimentally [26]. Including an onsite U at Ta does not cure this discrepancy, implying that these effects are beyond LDA+ U . Indeed, the strong \mathbf{T}_S -dependence of the electronic structure suggests that these deviations are related to the stacking disorder in the real material [20], which cannot be taken into account by our DFT-models. Notwithstanding these complications, our results indicate that 1T-TaS₂ may serve as a prime example for a pseudo-gap caused by a partially disordered electronic superlattice – an exciting new perspective, which certainly needs to be explored in the future.

In order to determine the origin of the dramatic effects of \mathbf{T}_S , we calculated the charge density distribution

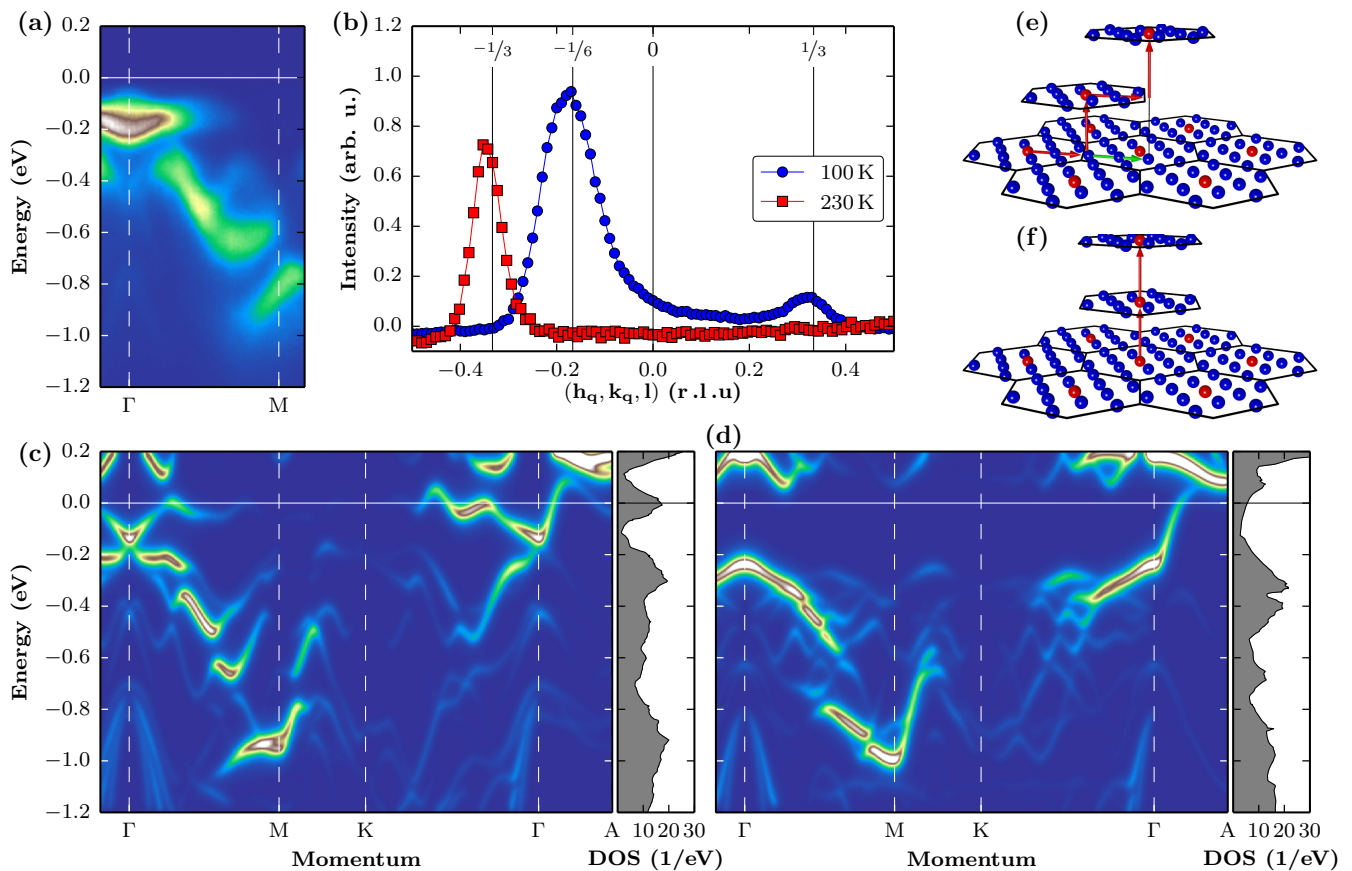


FIG. 2. **Different layer stackings and their impact on the band structure.** (c) and (d): Calculated band structure for the $2\mathbf{a} + \mathbf{c}$ -stacking and the \mathbf{c} -stacking, respectively. To facilitate the comparison with ARPES data shown in (a) the bandweights have been convoluted with a Lorentzian shaped resolution function. (e) and (f): Visualization of the $2\mathbf{a} + \mathbf{c}$ -stacking and \mathbf{c} -stacking, respectively. (b): XRD intensity measured along the l -direction for the C- and NC phase. The in-plane q -vector corresponds to $h_q = 17/13$, $k_q = 1/13$ for the C phase at 100 K and $h_q = 1.248$, $k_q = 0.068$ for the NC at 230 K. The single reflection observed for the NC-CDW implies a well-ordered stacking along c , fully consistent with previous results [17]. Upon entering the C-CDW phase, the XRD diffraction pattern changes dramatically and two broad peaks appear due to the presence of two metastable types of stackings (see text).

of the uppermost occupied states in real space. As can be seen in Fig. 3, for both stackings a complex orbital texture within the ab -plane emerges. This is the second major result of this work: the discovery of an orbital texture that is intertwined with a CDW. Note that not only the occupancy of a certain type of orbital changes spatially. Instead also the symmetry of the orbitals clearly changes from site to site, resulting in a complex orbital ordering pattern. For instance, whereas the orbital is oriented perpendicular to the ab -plane at the center of the Ta-cluster, a significant in-plane component exists at the cluster edges. It is also worth mentioning that the in-plane orientation of some orbitals changes with \mathbf{T}_S and that also the S 3p-states take part in the orbital texture.

The orbital structure for $\mathbf{T}_S = 1\mathbf{c}$ permits significant charge hopping only along c , as illustrated in Fig. 3 (e). In other words, the charges flow along orbital stripes along c , corresponding to the quasi one-dimensional character

of the uppermost band in Fig. 3 (a) and Fig. 2 (d). This drastically changes in the case of $\mathbf{T}_S = 2\mathbf{a} + \mathbf{c}$. Now there is a significant ab -component of the hopping as illustrated in Fig. 3 (f), so that the uppermost band attains a larger in-plane dispersion and crosses E_F along Γ -M and Γ -K (Figs. 3 (b) and 2 (c)).

These results have important consequences: Firstly, we find that the gap at Γ occurs already without including an onsite repulsion U on Ta. Instead, the band structure calculations reveal that this gap is for a large part due to the interlayer hybridization. The latter is in turn mostly caused by the $3z^2 - r^2$ -type orbitals pointing along c , i.e., the Γ -gap is directly coupled to the orbital texture. This result naturally explains the ultra-fast response of this gap observed in time-resolved ARPES experiments, since the disruption and reordering of the electronic orbitals can evolve on much faster time-scales than the lattice.

Secondly, the presence of orbital textures explains the

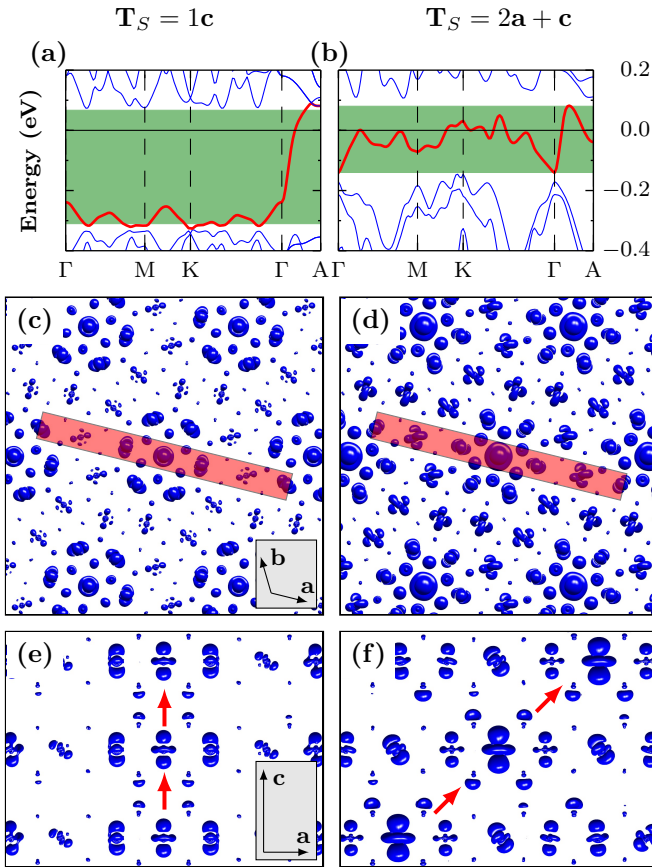


FIG. 3. **Real space illustration of the electron density for the highest occupied band.** (a) and (b): The band structure near E_F . The energy window used to calculate the energy-resolved electron density is indicated by the green area. (c) and (d): A complex orbital texture emerges within the ab -plane. (e): The $1c$ -stacking allows for significant hopping only along the c -direction. (f): A substantial ab -component of the hopping appears for the $2a + c$ -stacking.

strong pressure dependence of the CDW-order in $1T$ - TaS_2 , because through the orbital texture pressure has a large effect on the stability of CDW-phases with different stackings in a way that goes well beyond traditional nesting scenarios. We also stress that the crucial role of the interlayer interactions is verified experimentally by the data in Fig. (b), which shows that the stacking changes completely across the C-CDW/NC-CDW transition. This change in stacking together with our DFT-results also rationalizes the collapse of the gap at Γ upon entering the NC-CDW with warming.

Thirdly and most importantly, the relative orientation of the orbitals in adjacent ab -planes has a spectacular effect on the band dispersions. This can be readily understood in terms of the overlap integrals, which depend critically on the relative orientation of the orbitals in adjacent layers along c (cf. Figs. 2 (e),(f)). This immediately yields a new device concept, which employs metastable orbital orders for controlling the electronic structure of

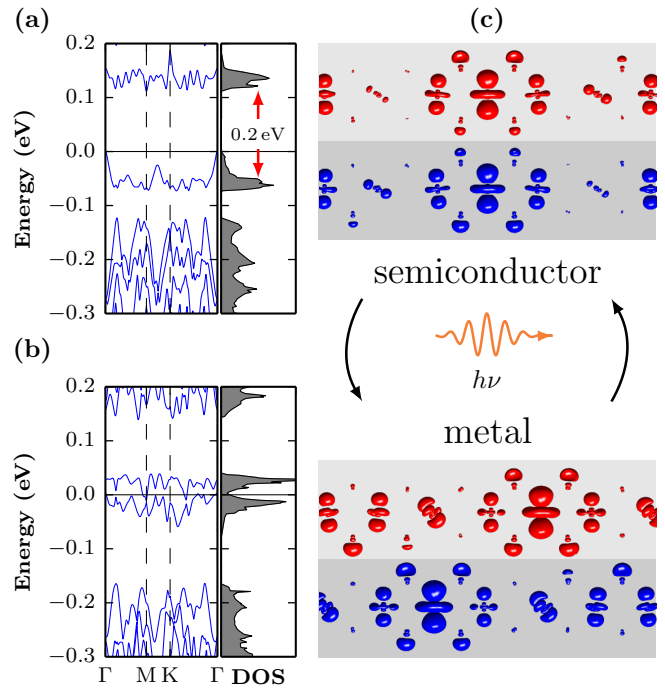


FIG. 4. **Device concept based on the switching between metastable orbital orders.** Calculated band structure for a bilayer of $1T$ - TaS_2 with $1c$ -stacking (a) and $2a + c$ -stacking (b). A semiconductor-to-metal transition takes place upon changing the stacking of the two layers. (c): Orbital order corresponding to the semiconducting (top) and metallic state (bottom). Recent experiments provide strong evidence that switching between these states is feasible on the femtosecond timescale [27].

nanostructures: As illustrated in Fig. 4 for a bilayer of $1T$ - TaS_2 , switching between the metastable orbital configurations causes a complete semiconductor-metal transition. In other words, by changing the orbital order in the direction *perpendicular* to the layers, one can control the conductivity *parallel* to the layers. Even though this effect has not yet been observed directly, a very recent experiment provides first evidence that this can be achieved reversibly and on ultra-fast timescales using optical laser pulses [27].

Orbital textures hence enable to manipulate the band dispersion and gap structure of $1T$ - TaS_2 in a very effective way. They therefore provide a new route to tailor and switch the electronic properties of TMDs, possibly on the femtosecond time scale. This concept of orbitronics may hence enable to create novel, small and ultra-fast electronics, which adds to the large potential of TMDs for future device applications.

This work was financially supported by the German Research Foundation under grant DFG-GRK1621. J.T and J.G gratefully acknowledge the financial support by the German Research Foundation through the Emmy Noether program (grant GE 1647/2-1). Y.I.J. and P.A.

were supported by U.S. Department of Energy grant DE-FG02-06ER46285. We thank K. Rossnagel for fruitful discussions.

METHODS

DFT

The DFT calculations were done using the FPLO14 package [28], which has been developed at the IFW Dresden and supports unfolding of the band structure as outlined in Ref. 24. Due to its small basis size it allows for calculations of large supercells extremely efficiently, which makes the presented calculations numerically affordable. The supercell structure for 1c-stacking was derived from reference 29 and 17. In order to simulate different layer stackings we transformed the hexagonal supercell into a triclinic supercell without changing the atomic displacements. It is important to note that a structural relaxation, which starts from the undistorted lattice, rapidly converges against the experimentally observed superstructure. This verifies our approach and shows that the present DFT-models capture the important interactions present in the real material.

XRD

XRD data were obtained at the beamline BW5 at the Deutsches Elektronensynchrotron (DESY). We mounted a high-quality single crystal of 1T-TaS₂ in a dispex Helium cryostat sitting in an Euler cradle. The presented XRD data was obtained by measuring the diffracted intensity of the superstructure reflection while scanning along the crystallographic *l*-direction for two different temperatures.

ARPES

ARPES measurements were conducted at the 1³-ARPES endstation at beamline UE112PG2 at the Berlin Synchrotron (BESSY). We used *p*-polarized light of 96 eV photon energy, so that the final state crystal momentum at normal emission corresponds to the Γ -point [30]. The sample temperature was kept at 1 K.

- [4] J. Chang, E. Blackburn, A. T. Holmes, N. B. Christensen, J. Larsen, J. Mesot, R. Liang, D. A. Bonn, W. N. Hardy, A. Watenphul, M. v. Zimmermann, E. M. Forgan, and S. M. Hayden, *Nat Phys* **8**, 871 (2012).
- [5] G. Ghiringhelli, M. Le Tacon, M. Minola, S. Blanco-Canosa, C. Mazzoli, N. B. Brookes, G. M. De Luca, A. Frano, D. G. Hawthorn, F. He, T. Loew, M. M. Sala, D. C. Peets, M. Salluzzo, E. Schierle, R. Sutarto, G. A. Sawatzky, E. Weschke, B. Keimer, and L. Braicovich, *Science* **337**, 821 (2012).
- [6] E. H. da Silva Neto, P. Aynajian, A. Frano, R. Comin, E. Schierle, E. Weschke, A. Gyenis, J. Wen, J. Schneeloch, Z. Xu, S. Ono, G. Gu, M. Le Tacon, and A. Yazdani, *Science* **343**, 393 (2014).
- [7] C. de la Cruz, Q. Huang, J. W. Lynn, J. Li, W. R. II, J. L. Zarestky, H. A. Mook, G. F. Chen, J. L. Luo, N. L. Wang, and P. Dai, *Nature* **453**, 899 (2010).
- [8] S. Mhlbauer, B. Binz, F. Jonietz, C. Pfleiderer, A. Rosch, A. Neubauer, R. Georgii, and P. Bni, *Science* **323**, 915 (2009).
- [9] Q. H. Wang, K. Kalantar-Zadeh, A. Kis, J. N. Coleman, and M. S. Strano, *Nature nanotechnology* **7**, 699 (2012).
- [10] M. Chhowalla, H. S. Shin, G. Eda, L.-J. Li, K. P. Loh, and H. Zhang, *Nature chemistry* **5**, 263 (2013).
- [11] B. Sipos, A. F. Kusmartseva, A. Akrap, H. Berger, L. Forro, and E. Tutis, *Nat Mater* **7**, 960 (2008).
- [12] P. Fazekas and E. Tosatti, *Philos. Mag. B* **39**, 229 (1979).
- [13] S. Hellmann, M. Beye, C. Sohrt, T. Rohwer, F. Sorgenfrei, H. Redlin, M. Kalläne, M. Marczyński-Bühlow, F. Hennies, M. Bauer, A. Föhlisch, L. Kipp, W. Wurth, and K. Rossnagel, *Phys. Rev. Lett.* **105**, 187401 (2010).
- [14] J. C. Petersen, S. Kaiser, N. Dean, A. Simoncini, H. Y. Liu, A. L. Cavalieri, C. Cacho, I. C. E. Turcu, E. Springate, F. Frassetto, L. Poletto, S. S. Dhesi, H. Berger, and A. Cavalleri, *Phys. Rev. Lett.* **107**, 177402 (2011).
- [15] L. Perfetti, P. A. Loukakos, M. Lisowski, U. Bovensiepen, H. Berger, S. Biermann, P. S. Cornaglia, A. Georges, and M. Wolf, *Phys. Rev. Lett.* **97**, 067402 (2006).
- [16] X. L. Wu and C. M. Lieber, *Science* **243**, 4899 (1989).
- [17] A. Spijkerman, J. L. de Boer, A. Meetsma, G. A. Wieggers, and S. van Smaalen, *Phys. Rev. B* **56**, 13757 (1997).
- [18] R. Ang, Y. Tanaka, E. Ieki, K. Nakayama, T. Sato, L. J. Li, W. J. Lu, Y. P. Sun, and T. Takahashi, *Phys. Rev. Lett.* **109**, 176403 (2012).
- [19] S. Tanda, T. Sambongi, T. Tani, and S. Tanaka, *Journal of the Physical Society of Japan* **53**, 476 (1984).
- [20] K. Nakanishi and H. Shiba, *Journal of the Physical Society of Japan* **53**, 1103 (1984).
- [21] M. Bovet, S. van Smaalen, H. Berger, R. Gaal, L. Forró, L. Schlapbach, and P. Aebi, *Phys. Rev. B* **67**, 125105 (2003).
- [22] P. Darancet, A. J. Millis, and C. A. Marianetti, *Phys. Rev. B* **90**, 045134 (2014).
- [23] A. Damascelli, Z. Hussain, and Z.-X. Shen, *Rev. Mod. Phys.* **75**, 473 (2003).
- [24] W. Ku, T. Berlijn, and C.-C. Lee, *Phys. Rev. Lett.* **104**, 216401 (2010).
- [25] K. Rossnagel, *J. Phys.: Condens. Matter* **23**, 213001 (2011).
- [26] T. Pillo, J. Hayoz, H. Berger, M. Grioni, L. Schlapbach, and P. Aebi, *Phys. Rev. Lett.* **83**, 3494 (1999).

-
- [1] Y. Zhang, Y.-W. Tan, H. L. Stormer, and P. Kim, *Nature* **438**, 201 (2005).
 - [2] A. Ohtomo and H. Y. Hwang, *Nature* **427**, 423 (2004).
 - [3] G. Grüner, *Density waves in solids*, Vol. 89 (Addison-Wesley Reading, MA, 1994).

- [27] L. Stojchevska, I. Vaskivskiy, T. Mertelj, P. Kusar, D. Svetin, S. Brazovskii, and D. Mihailovic, *Science* **344**, 177 (2014).
- [28] K. Koepnik and H. Eschrig, *Phys. Rev. B* **59**, 1743 (1999).
- [29] R. Brouwer, *Incommensurability in crystal structures*, Ph.D. thesis, Rijksuniversiteit Groningen (Netherlands) (1978).
- [30] K. Rossnagel, E. Rotenberg, H. Koh, N. V. Smith, and L. Kipp, *Phys. Rev. Lett.* **95**, 126403 (2005).